Ab initio relativistic calculation of the RbCs molecule

S. Kotochigova[a)]
Department of Physics, Temple University, Philadelphia, Pennsylvania 19122 and National Institute of Standards and Technology, 100 Bureau Drive, Stop 8423, Gaithersburg, Maryland 20899

E. Tiesinga
National Institute of Standards and Technology, 100 Bureau Drive, Stop 8423, Gaithersburg, Maryland 20899

(Received 27 July 2005; accepted 6 September 2005; published online 28 October 2005)

We apply the relativistic configuration-interaction valence-bond method to calculate various characteristics of the alkali-metal RbCs dimer. These include the electronic potentials and transition dipole moments between the ground and first excited states and permanent dipole moments of the $X\,^1\Sigma^+$ and $a\,^3\Sigma^+$ states of the ground configuration. In addition, we estimate the lifetime of the rovibrational levels of the X state due to blackbody radiation. These data can help experimentalists to optimize photoassociative formation of ultracold RbCs molecules and their longevity in a trap or in an optical lattice. Extended basis sets, constructed from Dirac-Fock and Sturm's orbitals, have been used to ensure convergence of our calculations. We compare our data with other theoretical and experimental results when they were available. © *2005 American Institute of Physics*.
[DOI: 10.1063/1.2107607]

I. INTRODUCTION

We perform an *ab initio* relativistic valence-bond study of the heteronuclear alkali-metal RbCs molecule, critical for a physical realization of highly controlled molecular systems. Placed in an optical lattice ultracold alkali-metal molecules in general and RbCs molecules, in particular, can form addressable coherent qubits, possibly leading to the creation of scalable quantum information devices.[1] Such arrays of trapped and ultracold molecules might be used for the modeling of condensed-matter systems and chemical reactions.[2] Experimental work towards the cooling and creation of heteronuclear molecules is now being actively pursued by several experimental groups (see, for example, Refs. 1 and 3–6).

Alkali-metal molecules are the most relevant for studies of cold molecules because the constituent atoms can be laser cooled and trapped, individually, and photoassociated to form a stable bond. In particular, efficient production of alkali-metal molecules might occur by a two-photon stimulated Raman photoassociation (PA) transition.[7–11] Two colliding ground-state atoms absorb a photon with energy $h\nu$ to create an excited molecule. A second laser transfers this state, by stimulated emission, into a single rotational and vibrational state of the ground configuration. These ground-state molecules are expected to have a temperature comparable to that of the atoms from which they are formed. Detailed calculations of the ground and excited potential surfaces and of the transition and permanent dipole moments are necessary to coordinate experimental efforts to form ultracold molecules in stable rovibrational levels of the ground-state configuration.

We are interested in the properties of electronic states of RbCs dissociating to the ground Rb $5s\,(^2S_{1/2})$ +Cs $6s\,(^2S_{1/2})$ and excited Rb $5s\,(^2S_{1/2})$+Cs $6p\,(^2P_{1/2})$ asymptotes. Accurate knowledge of excited RbCs potentials and the transition dipole moments between the ground and excited states for different internuclear separations will help experimentalists to design stimulated Raman steps that are optimized for a high molecular production rate to, for example, the $v=0$ vibrational level of the $X\,^1\Sigma^+$ state.

For RbCs the theoretical information on potential-energy curves, presently available, is contradictory.[12–14] Calculations performed in Refs. 12 and 13 are not adequate, since they do not include the spin-orbit effects crucial for a precise understanding of such a heavy molecule as RbCs. Our *ab initio* relativistic calculation will take into account the spin-orbit interaction nonperturbatively, producing realistic molecular potentials. A detailed comparison with pseudopotential calculations of Fahs *et al.*,[14] who included the spin-orbit interaction, will be presented.

For the transition dipole moments the usage of the relativistic approach is essential as it predicts nonzero dipole moments for transitions between nominal singlet and triplet states. To our knowledge, the transition dipole moments between the ground and first excited states of RbCs have never been determined either theoretically or experimentally. Experimentally it is often hard to obtain absolute measurements of photoassociative transition rates. To interpret experimental data and design experiments to produce cold molecules, *ab initio* calculations are then required.

In a heteronuclear molecule, such as RbCs, the electrons are distributed unequally between the two nuclei, creating a permanent dipole moment. It is our goal to calculate the permanent dipole moments of the ground-state $X\,^1\Sigma^+$ and $a\,^3\Sigma^+$ potentials as function of internuclear separation R. These dipole moments will allow us to evaluate the lifetime of the RbCs molecule in the presence of blackbody radiation

[a)]Electronic mail: svetlana.kotochigova@nist.gov

from the surrounding room-temperature surfaces present in any laser cooling experiment. In addition, the strength of the permanent dipole moment directly determines the strength of the dipole-dipole force between polar molecules as they are held in an optical lattice.

The permanent dipole moment of the $X\,^1\Sigma^+$ state in RbCs has been calculated by Ref. 15 for a single R value, the equilibrium distance R_e, using an *ab initio* pseudopotential configuration-interaction method. Recently, Aymar and Dulieu[16] published a theoretical calculation of the permanent dipole moments of several heteronuclear alkali-metal dimers, including RbCs. They applied a pseudopotential approach using a Gaussian basis set and combined it with a self-consistent-field configuration-interaction method. We will present permanent dipole moments obtained with our relativistic *ab initio* valence-bond theory. We feel that it is beneficial to compare our data with those existing in the literature as it is hard for any theoretical method to gauge its accuracy. Thus, a comparison will allow us to more confidently estimate the theoretical uncertainties.

We use the relativistic configuration-interaction valence-bond (RCI-VB) method for all our calculations. It naturally includes the spin-orbit interaction, an essential element for describing the coupling and nonzero transition dipole moments between singlet and triplet potentials. The valence-bond method is a suitable tool for the study of electronic properties of molecules formed by colliding atoms as VB molecular wave functions are constructed from atomic wave functions localized at the different atomic centers. For large internuclear separations the molecular wave function obtains a pure atomic form, which is the correct asymptotic limit for any molecular function. We have already applied the RCI-VB method to the heavy noble-gas Xe_2 molecule,[17] the alkali-metal molecules Rb_2 and Cs_2,[18] the polar KRb molecule,[19] and alkaline-earth dimers.[20,21]

Initiated by experimental efforts to form ultracold RbCs by photoassociation, Bergeman *et al.*[10] have partially analyzed RbCs spectral data obtained at the Laboratoire Aimé Cotton (Ref. 22) a few years ago. Additional information on RbCs would be useful in understanding unresolved problems in the analysis of the observed spectra. We would like to point out that the experiments with RbCs face the difficulty that the energy-level structure of the lowest $^{1,3}\Sigma^+$ and $^{1,3}\Pi$ excited states is known inadequately. Moreover, these states are mixed by strong spin-orbit coupling, and to date, these perturbations have not been systematically analyzed.

Sections II and III discuss the relativistic configuration-interaction valence-bond method as our study relies heavily on its strengths. We describe among other things the construction of localized atomic orbitals used as basis functions in the molecular calculation. Primary attention is given to the introduction of the lesser known numerical Sturm functions and their advantages for the description of virtual molecular orbitals. In Sec. IV we present results obtained for the RbCs molecule in the form of electronic potential surfaces and permanent and transition dipole moments as a function of internuclear separation. We also calculate the rovibrational levels of the ground $X\,^1\Sigma^+$ state and determine their lifetime due to blackbody radiation. Some of our data we have compared with other research in the literature. Tables of potential-energy values and permanent and transition dipole moments of RbCs versus internuclear separation can be found through EPAPS.[23]

II. THEORY

A. Relativistic Dirac-Fock and Sturm basis functions

An important feature of our RCI-VB approach is the use of numerical relativistic Dirac-Fock and Sturm single-electron atomic wave functions or orbitals for the construction of the molecular basis functions. This version of the VB method has been described earlier in Refs. 17 and 24. Since both references were published in hard to obtain publications we repeat some of the formalism here. In the VB method atomic Dirac-Fock functions describe occupied orbitals of the constituent atoms and Sturm functions serve as a basis set for unoccupied orbitals. Single-electron Dirac-Fock functions are obtained by solving the integrodifferential Dirac-Fock equations self-consistently for each of the atoms in the molecule. These equations are derived by applying the conventional Hartree-Fock method to the relativistic many-body Hamilton operator

$$\hat{H} = \sum_i \hat{h}_i + \sum_{i<j} \hat{v}_{ij} \tag{1}$$

for each atom. Here $\hat{h}_i = c(\boldsymbol{\alpha}_i \cdot \mathbf{p}_i) + \beta_i c^2 - Z/r_i$ is the Dirac operator for electron i in the Coulomb field of a nucleus with positive charge Z. The quantities α_i and β_i are the Dirac matrices, the vector $\mathbf{p}_i$ is the momentum of electron i, $\mathbf{r}_i$ is the location of electron i relative to the nucleus of the atom, and c is the speed of light. The operator $\hat{v}_{ij} = 1/|\mathbf{r}_i - \mathbf{r}_j|$ is the Coulomb operator between electrons i and j. We have expressed all operators and variables in a.u. The a.u. of energy is a hartree, $E_h = 4.359\,744 \times 10^{-18}$ J, and the a.u. of length is a bohr, $1a_0 = 0.052\,917\,7$ nm. The speed of light is 137.036 in a.u.

In the central-field approximation the single-electron Dirac-Fock orbital is a four-component Dirac spinor[25]

$$\psi_{n\kappa\mu}(\mathbf{r}) = \frac{1}{r}\begin{pmatrix} P_{n\kappa}(r) & \chi_{\kappa\mu}(\theta,\vartheta) \\ iQ_{n\kappa}(r) & \chi_{-\kappa\mu}(\theta,\vartheta) \end{pmatrix} \tag{2}$$

and has an energy $\epsilon_{n\kappa}$. The radial functions $P_{n\kappa}(r)$ and $Q_{n\kappa}(r)$ are the large and small components of the radial wave function, respectively; $\chi_{\kappa\mu}(\theta,\vartheta)$ is the angular Dirac spinor, labeled by $\kappa = \ell(\ell+1) - (j+1/2)^2$, where ℓ and j are the orbital and total angular momentum quantum numbers, and μ is the projection quantum number of j. The label n is the principal quantum number where for fixed κ the energy $\epsilon_{n\kappa}$ increases with increasing n. The Lagrange multiplier formalism has been used to ensure that $\psi_{n\kappa\mu}$ with different principal quantum number but the same $\kappa\mu$ are orthogonal. Instead of using the relativistic κ notation we often prefer to use the equivalent notations lj or l_j to describe orbitals. Moreover, to good approximation n can be thought of as counting the number of nodes plus one of the large components of the Dirac spinor.

The radius of the Dirac-Fock orbitals grows rapidly with the level of excitation, i.e., the principal quantum number n.

Consequently, the spatial overlap between orbitals becomes progressively smaller, and the use of these orbitals in configuration interactions is not practical as the convergence of the eigenvalues with increasing number of orbitals is slow. An alternative to the Dirac-Fock orbitals is the use of so-called Sturm functions.[26–30] Sturm orbitals are obtained by solving Dirac-Fock-Sturm equations

$$[H_{\mathrm{DF}} - \varepsilon_{0\kappa}]\phi^{\mathrm{DFS}}_{n\kappa\mu}(\mathbf{r}) = \lambda_{n\kappa} W_{\kappa}(r)\phi^{\mathrm{DFS}}_{n\kappa\mu}(\mathbf{r}), \tag{3}$$

where H_{DF} is a Dirac-Fock operator, $\lambda_{n\kappa}$ is the eigenvalue of the Sturm orbital $n\kappa\mu$, and the energy $\varepsilon_{0\kappa}$ is fixed for each orbital with the same value of κ and μ. The functions $W_{\kappa}(r)$ are weight functions that approach zero for large r. Consequently, for large r all Sturm orbitals with the same κ have a radial behavior solely determined by $\varepsilon_{0\kappa}$. In other words, Sturm orbitals with the same κ have approximately the same radius. Note that Eq. (3) forms a Hermitian operator with a complete but discrete set of eigenfunctions.

In a typical configuration-interaction calculation a combination of Dirac-Fock and Sturm orbitals is used and the energies $\varepsilon_{0\kappa}$ in the Dirac-Fock-Sturm equations are set equal to a Dirac-Fock orbital $n\kappa\mu$. In this case $\lambda_{n\kappa}=0$ is an eigenvalue of the Dirac-Fock-Sturm equations and the corresponding Sturm functions are equal to the corresponding DF orbitals. For the eigenvalues $\lambda_{n\kappa}>0$ we label the Sturm functions according to the values κ and μ of the DF orbital and $n' > n$ increasing for increasing $\lambda_{n\kappa}$.

We have chosen the weight functions

$$W_{\kappa}(r) = -\frac{1-\exp[-(\zeta_{\kappa}r)^2]}{(\zeta_{\kappa}r)^2}. \tag{4}$$

For $\zeta_{\kappa}r \ll 1$ the weight function approaches unity while for $\zeta_{\kappa}r \gg 1$ it approaches zero as $1/r^2$ faster than a Coulomb potential. The parameters ζ_{κ} are chosen to ensure that the $W_{\kappa}(r)$ are approximately constant in the vicinity of the atomic core and do not distort the DF core orbitals.

Figure 1 shows some of the Dirac-Fock and Sturm orbitals of the rubidium atom. For this calculation the $1s$, $2s$, $2p_j$, $3s$, $3p_j$, $3d_j$, $4s$, $4p_j$, $4d_j$, and $5s$ orbitals of Rb are Dirac-Fock orbitals and obtained from the self-consistent Dirac-Fock equations. Only the $5s$ ($\kappa=-1$) orbital is shown in Fig. 1. The virtual $6s$ and $7s$ orbitals can be constructed as either Dirac-Fock or Sturm functions and are shown in Fig. 1. The radii of the $6s$ and $7s$ Dirac-Fock orbitals are significantly larger than that of the $5s$ orbital, while the corresponding Sturm orbitals remain localized. The two Sturm orbitals are solved using the energy of the $5s$ Dirac-Fock orbital.

We also find it useful to denote many-electron atomic configurations by $(n_1 l_1 j_1)^{q_1}\cdots(n_A l_A j_A)^{q_A}$, where A is the number of shells with nonzero occupancy, q_i is the number of electrons in this shell, and nlj denotes one of the Dirac-Fock or Dirac-Fock-Sturm orbitals $nlj\mu$. Each configuration encompasses multiple atomic Slater determinants. For each determinant the projections μ are also specified.

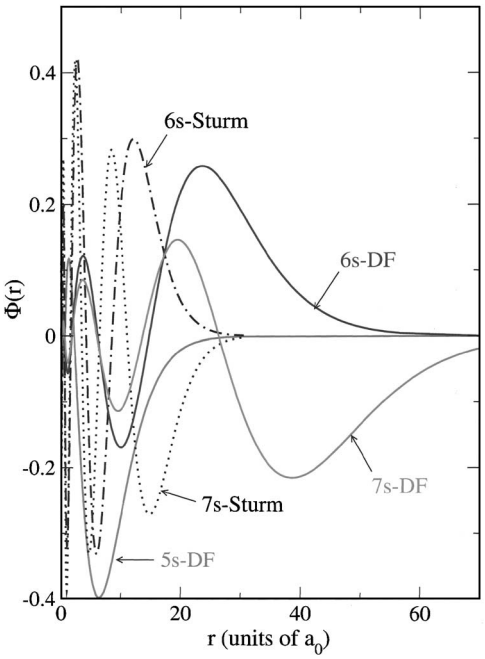

FIG. 1. Dirac-Fock (solid lines) and Sturm (dotted and dashed-dotted lines) s-wave functions of atomic Rb.

B. Molecular wave functions

The molecular wave functions are constructed from atomic orbitals localized at the different atomic centers A and B by

$$\Psi_{AB} = \sum_{\alpha} C_{\alpha} \det{}^{AB}_{\alpha}, \tag{5}$$

where $\det^{AB}_{\alpha}$ is a many-electron molecular Slater determinant, constructed as an antisymmetrized product of two atomic Slater determinants. The configuration-interaction (CI) coefficients C_{α} are obtained by solving the generalized eigenvalue matrix problem

$$\hat{H}_{AB}\mathbf{C} = E\hat{S}_{AB}\mathbf{C}, \tag{6}$$

where $\hat{H}_{AB}$ is the CI Hamiltonian matrix for the molecule. The nonorthogonality matrix $\hat{S}_{AB}$ is the overlap matrix of molecular Slater determinants calculated by

$$(\hat{S}_{AB})_{\alpha\beta} = \langle \det{}^{AB}_{\alpha} | \det{}^{AB}_{\beta} \rangle = (D_{\alpha\alpha}D_{\beta\beta})^{-1/2} D_{\alpha\beta}, \tag{7}$$

where $D_{\alpha\beta}=\det|\langle\alpha_i|\beta_j\rangle|$ is the determinant of overlap integrals $S^{\alpha\beta}_{i,j}=\langle\alpha_i|\beta_j\rangle$ between the single-electron orbitals α_i and β_j belonging to Slater determinants $\det^{4B}_{\alpha}$ and $\det^{AB}_{\beta}$, respectively. Each orbital $\alpha_i(\beta_j)$ stands for a four-component atomic orbital $\psi_{n\kappa}(\mathbf{r})$ centered at either nucleus A or B. All determinants $\det^{AB}_{\alpha}$ contain N orbitals, where N is the number of electrons in the molecule.

At small internuclear separations R one-electron orbitals located around different centers have considerable overlap, that is, are nonorthogonal. This gives rise to a large exchange interaction and thereby creates the bond. For large internuclear separations the molecular wave function automatically obtains a pure atomic form and therefore correctly dissociates. Herein lies the uniqueness of the VB method and the

relevance for cold-atomic and molecular physics. An alternative approach, such as the molecular-orbital theory, uses as a starting point molecular orbitals, containing two electrons, which are a poor approximation for the large R.

Our approach is, in principle, an all-electron calculation, which, for instance, allows us to evaluate the electronic densities at the nuclear sites and to calculate hyperfine-structure constants. Hence, the dynamics of all electrons in a molecule is accounted for. However, often this is not necessary. Deeply-lying orbitals do not take part in the molecular formation. Therefore, we introduce core and valence orbitals where core electrons will not participate in the CI. The method is designed to calculate the electronic potential surfaces and other electronic properties of dimers composed of atoms with any nuclear charge Z, any number of electrons, and any level of excitation.

An important contribution to molecule formation arises from ionic configurations, in which the participating atoms are positively and negatively charged, respectively. The presence of ionic configurations leads to the deformation of the atomic wave functions and hence to a more realistic description of a molecule. These configurations will also be one of the determining factors in the accuracy of the dipole moment calculations of the RbCs polar molecule.

The Hamiltonian matrix $\hat{H}_{AB}$ contains one- and two-electron contributions and the Coulomb repulsion u_{AB} between the nuclei and is evaluated via

$$(\hat{H}_{AB})_{\alpha\beta} = \langle \det_\alpha^{AB} | \sum_{i=1}^{N} \hat{h}_i + \sum_{i<j}^{N} \hat{v}_{ij} + u_{AB} | \det_\beta^{AB} \rangle, \tag{8}$$

where the one-electron matrix elements are obtained in the form

$$\langle \det_\alpha^{AB} | \sum_{i=1}^{N} \hat{h}_i | \det_\beta^{AB} \rangle = (D_{\alpha\alpha} D_{\beta\beta})^{-1/2} D_{\alpha\beta} \times \sum_{i,j=1}^{N} (S^{-1})_{i,j}^{\alpha,\beta} \langle \alpha_i | \hat{h} | \beta_j \rangle, \tag{9}$$

where

$$\hat{h} = c(\boldsymbol{\alpha}\mathbf{p}) + \beta c^2 - \frac{Z_A}{|\mathbf{r} - \mathbf{R}_A|} - \frac{Z_B}{|\mathbf{r} - \mathbf{R}_B|}, \tag{10}$$

and R_A and R_B are the nuclear coordinates. Two-electron matrix elements are obtained in the form

$$\langle \det_\alpha^{AB} | \sum_{i<j}^{N} \hat{v}_{ij} | \det_\beta^{AB} \rangle = (D_{\alpha\alpha} D_{\beta\beta})^{-1/2} \sum_{i,k=1}^{N} \sum_{j,l=1}^{N} D_{i,j,k,l}^{\alpha\beta} \times \langle \alpha_i, \alpha_j | \frac{1}{r_{12}} | \beta_k, \beta_l \rangle, \tag{11}$$

where

$$D_{i,j,k,l}^{\alpha\beta} = D_{\alpha\beta} \varepsilon_{i,k} \varepsilon_{j,l} [(S^{-1})_{i,j}^{\alpha,\beta} (S^{-1})_{k,l}^{\alpha,\beta} - (S^{-1})_{i,l}^{\alpha\beta} (S^{-1})_{k,j}^{\alpha\beta}]. \tag{12}$$

$\varepsilon_{i,k} = 1$ for $i<k$ and -1 for $i>k$, and the evaluation of the matrix elements $\langle \alpha_i | \hat{h} | \beta_j \rangle$ and $\langle \alpha_i, \alpha_j | 1/r_{12} | \beta_k, \beta_l \rangle$ will be discussed in Sec. III.

It is convenient to define one- and two-particle density transition matrices between determinants $\det_\alpha^{AB}$ and $\det_\beta^{AB}$. The one-particle density matrix is given by

$$\rho_1^{\alpha,\beta}(\mathbf{r}, \mathbf{r}') = (D_{\alpha\alpha} D_{\beta\beta})^{-1/2} D_{\alpha\beta} \sum_{i,j}^{N} (S^{-1})_{i,j}^{\alpha,\beta} \psi_i(\mathbf{r}) \psi_j^*(\mathbf{r}'), \tag{13}$$

where $\psi_i(\mathbf{r})$ and $\psi_j^*(\mathbf{r}')$ are the atomic orbitals and the two-particle density matrix is

$$\rho_2^{\alpha,\beta}(\mathbf{r}_1, \mathbf{r}_2 | \mathbf{r}_1', \mathbf{r}_2') = (D_{\alpha\alpha} D_{\beta\beta})^{-1/2} \sum_{i \neq k}^{N} \sum_{j \neq l}^{N} D_{i,j,k,l}^{\alpha,\beta} \times \psi_i(\mathbf{r}_1) \psi_j^*(\mathbf{r}_1') \psi_k(\mathbf{r}_2) \psi_l^*(\mathbf{r}_2'). \tag{14}$$

III. ONE- AND TWO-ELECTRON MATRIX ELEMENTS

One- and two-electron Hamiltonian matrix elements, $\langle \alpha_i | \hat{h} | \beta_j \rangle$ and $\langle \alpha_i, \alpha_j | 1/r_{12} | \beta_k, \beta_l \rangle$, and matrix elements $S_{i,j}^{\alpha\beta}$ are calculated using a modified Löwdin's reexpansion procedure.[31] We expand atomic orbitals located around one of the atomic centers onto the other center. The modification concerns the fact that Löwdin's method is not very efficient when expanding strongly localized orbitals. In the modified approach the integration region is divided into two and in each region only the slowly varying part of the basis function centered in the other region is expanded. This symmetric expansion has much faster convergence characteristics than the method proposed in Ref. 31.

We only apply the reexpansion procedure to the "tails" of wave functions occurring in a given region. To be more precise the range of integration is divided into two exclusive regions V_A and V_B, where region V_A contains atom A and the region V_B contains atom B. After introducing the step function $\Theta_\tau(\mathbf{r}) = 1$ for $\mathbf{r} \in V_\tau$ and 0 otherwise, where $\tau = A$ or B, the part of a single-electron orbital centered at B but located in V_A can be expanded around center A as

$$\Theta_A(\mathbf{r}) \frac{f_b(|\mathbf{r}_B|)}{|\mathbf{r}_B|} \chi_{\kappa_b \mu_b}(\hat{r}_B) = \frac{1}{r_A} \sum_{\kappa} \zeta_b(A, \kappa\mu_b | r_A) \chi_{\kappa\mu_b}(\hat{r}_A), \tag{15}$$

where f_b is either the large $P_{n_b\kappa_b}$ or small $Q_{n_b-\kappa_b}$ component of a four-component spinor, $\mathbf{r}_\tau = \mathbf{r} - \mathbf{R}_\tau$ for $\tau = A$ or B, $\mathbf{r}$ is the location of the electron, and R_τ are the locations of the atomic nuclei. The expansion coefficients ζ_b are given by

$$\zeta_b(A,\kappa\mu_b|r_A)=\sum_{m,\sigma}C^{j_b\mu_b}_{\ell_b m(1/2)\sigma}C^{j\mu_b}_{\ell m,(1/2)\sigma}\frac{K_{\ell m}K_{\ell_b m}}{R}\times\int_{\max(|r_A|,|R-r_A|)}^{|R+r_A|}dr_B f_b(r_B)\times P^{|m|}_{\ell_b}\left(\left|\frac{r_B^2+R^2-r_A^2}{2r_BR}\right|\right)\times P^{|m|}_{\ell}\left(\left|\frac{r_A^2+R^2-r_B^2}{2r_BR}\right|\right),\tag{16}$$

where $\kappa_b\leftrightarrow l_b j_b$, $\kappa\leftrightarrow lj$, $R=|\mathbf{R}_A-\mathbf{R}_B|$, $C^{j\mu}_{\ell m\ell' m'}$ are Clebsch-Gordan coefficients, $P^{|m|}_{\ell}$ are the associated Legendre polynomials, $\sigma=m-\mu$, and

$$K_{\ell m}=\sqrt{\frac{(2\ell+1)}{2}\frac{(\ell-|m|)!}{(\ell+|m|)!}}.$$

Using Eq. (16) the overlap integral $S^{\alpha\beta}_{i,j}$ between orbital α_i of $\det^{AB}_{\alpha}$, centered around nucleus A, and β_j of $\det^{AB}_{\beta}$, centered around nucleus B, is

$$S^{\alpha\beta}_{i,j}=\int_0^\infty dr\{P_{n_a\kappa_a}(r)\zeta_{n_b\kappa_b}(A,\kappa_a\mu_a|r_A)+P_{n_b\kappa_b}(r)\zeta_{P_a}(B,\kappa_b\mu_b|r_B)\}+\int_0^\infty dr\{Q_{n_a\kappa_a}(r)\zeta_{n_b\kappa_b}\times(A,-\kappa_a\mu_a|r_A)+Q_{n_b\kappa_b}(r)\zeta_{n_a\kappa_a}(B,-\kappa_b\mu_b|r_B)\},\tag{17}$$

where orbital α_i has quantum numbers $n_a\kappa_a\mu_a$ and β_j has quantum numbers $n_b\kappa_b\mu_b$.

A. Coulomb-type two-center integrals

The reexpansion procedure for the calculation of matrix elements of the electron-electron Coulomb interaction requires additional attention. This subsection looks in detail at the Coulomb-type integrals while the next subsection looks at exchange-type integrals. Coulomb-type integrals are of the form

$$\gamma_{ac,bd}=\int d\mathbf{r}_1\int d\mathbf{r}_2\frac{\rho_{a,c}(\mathbf{r}_{1A})\rho_{b,d}(\mathbf{r}_{2B})}{|\mathbf{r}_1-\mathbf{r}_2|},\tag{18}$$

where $\rho_{ac}(\mathbf{r}_{1A})=\psi^*_a(\mathbf{r}_{1A})\psi_c(\mathbf{r}_{1A})$ and $\rho_{bd}(\mathbf{r}_{2B})=\psi^*_b(\mathbf{r}_{2B})\psi_d(\mathbf{r}_{2B})$ are the densities of products of four-component electronic wave functions centered at A and B, respectively. The coordinates are defined as $\mathbf{r}_{i\tau}=\mathbf{r}_i-\mathbf{R}_\tau$ for electron coordinate $\mathbf{r}_i(i=1,2)$ and nuclear coordinate $\mathbf{R}_\tau$ ($\tau=A,B$). Since the Coulomb potential for a test charge in the presence of a charge density ρ is

$$U(\mathbf{r})=\int d\mathbf{r}'\frac{\rho(\mathbf{r}')}{|\mathbf{r}-\mathbf{r}'|},$$

the Coulomb matrix elements, Eq. (18), can be written as

$$\gamma_{ac,bd}=\int d\mathbf{r}_2U_{ac}(\mathbf{r}_{2A})\rho_{bd}(\mathbf{r}_{2B}).\tag{19}$$

The density $\rho_{bd}(\mathbf{r})$ and Coulomb potentials $U_{ac}(\mathbf{r})$ can be expanded in terms of spherical harmonics $Y_{\ell m}$. For $\rho_{bd}(\mathbf{r})$ we have

$$\rho_{bd}(\mathbf{r})=\frac{1}{r^2}\sum_{\ell,m}\rho^\ell_{bd}(r)Y_{\ell m}(\hat{r})=\frac{1}{r^2}\sum_{\ell,m}\sqrt{\frac{2\ell+1}{4\pi}}g^\ell(j_b\mu_b,j_d\mu_d)Y_{\ell m}(\hat{r})\rho_{bd}(r),$$

where $g^\ell(j\mu,j'\mu')$ are the relativistic Gaunt coefficients

$$g^\ell(j\mu,j'\mu')=\frac{\sqrt{(2j+1)(2j'+1)}}{2\ell+1}(-1)^{\mu'+(1/2)}\times C^{\ell,\mu-\mu'}_{j\mu,j'-\mu'}C^{\ell,0}_{j-(1/2),j'-(1/2)},$$

and $\rho_{bd}(r)$ is the radial electronic density

$$\rho_{bd}(r)=P_b(r)P_d(r)+Q_b(r)Q_d(r).\tag{20}$$

The potential $U_{ac}(\mathbf{r})$ is expanded as

$$U_{ac}(\mathbf{r})=\frac{1}{r}\sum_\ell v^\ell_{ac}(r)Y_{\ell\mu}(\hat{r}),\tag{21}$$

where

$$v^k_{ac}(r)=\sqrt{\frac{4\pi}{2k+1}}g^k(j_a\mu_a,j_c\mu_c)r\int dr'\rho^k_{ac}(r')\frac{(r_<)^k}{(r_>)^{k+1}},$$

and

$$\frac{1}{|\mathbf{r}-\mathbf{r}'|}=4\pi\sum_{k=0}^\infty\frac{1}{2k+1}r^k_</r^{k+1}_>\sum_\mu Y_{k\mu}(\hat{r})Y^*_{k\mu}(\hat{r}'),$$

and $r_>(r_<)$ is the larger (smaller) of r' and r.

The integration region of $\mathbf{r}$ in Eq. (19) is divided into integration regions V_A and V_B and the surface S between V_A and V_B. That is, we rewrite Eq. (19) as

$$\gamma_{ac,bd}=\gamma^{(V_A)}_{ac,bd}+\gamma^{(V_B)}_{ac,bd}+\gamma^{(S)}_{ac,bd},\tag{22}$$

where

$$\gamma^{(V_A)}_{ac,bd}=\int_{V_A}d\mathbf{r}U_{ac}(\mathbf{r}_A)\rho_{bd}(\mathbf{r}_B),$$

$$\gamma^{(V_B)}_{ac,bd}=\int_{V_B}d\mathbf{r}U_{bd}(\mathbf{r}_B)\rho_{ac}(\mathbf{r}_A),$$

$$\gamma^{(S)}_{ac,bd}=-\frac{1}{4\pi}\int_S dS\left[U_{ac}(\mathbf{r}_A)\frac{\partial}{\partial z}U_{bd}(\mathbf{r}_B)-U_{bd}(\mathbf{r}_B)\frac{\partial}{\partial z}U_{ac}(\mathbf{r}_A)\right],\tag{23}$$

and we have used the Laplace equation $\Delta U(\mathbf{r})=-4\pi\rho(\mathbf{r})$ and applied Green's theorem in the integration over the surface S. The three quantities in Eqs. (23) can now be evaluated by a symmetrical expansion procedure of the densities

$\Theta_A(\mathbf{r}_B)\rho_{bd}(\mathbf{r}_B)$ and $\Theta_B(\mathbf{r}_A)\rho_{ac}(\mathbf{r}_A)$, obtained in a manner analogous to that for Eq. (15).

B. Exchange-type integrals

An exchange-type interaction matrix element has the form

$$h_{ac,bd} = \int\int d\mathbf{r}_1 d\mathbf{r}_2 \psi_a^*(\mathbf{r}_{1A})\psi_b(\mathbf{r}_{1B})\frac{1}{r_{12}}\psi_c(\mathbf{r}_{2A})\psi_d^*(\mathbf{r}_{2B}), \tag{24}$$

where the single-electron four-component wave functions labeled by a and c are centered at A and those labeled by b and d are centered at B. The spatial integrations is divided in four parts via

$$\int\int d\mathbf{r}_1 d\mathbf{r}_2 = \left(\int_{V_A} d\mathbf{r}_1 + \int_{V_B} d\mathbf{r}_1\right)\left(\int_{V_A} d\mathbf{r}_2 + \int_{V_B} d\mathbf{r}_2\right),$$

where the half planes $V_{A,B}$ are as before. Hence, the exchange-type integral has the four contributions

$$h_{ac,bd} = h_{ac,bd}^{(AA)} + h_{ac,bd}^{(BB)} + h_{ac,bd}^{(AB)} + h_{ac,bd}^{(BA)}, \tag{25}$$

where the first two terms correspond to integrals where the electrons are in the same spatial region and the last two terms are related to integrals where the electrons are in mutually exclusive spatial regions. Each contribution of this exchange-type integral has a contribution from the large component P and small component Q. That is,

$$h_{ac,bd}^{\tau\tau'} = h_{ac,bd}^{P,(\tau\tau')} + h_{ac,bd}^{Q,(\tau\tau')} \tag{26}$$

for τ, $\tau' = A$ or B. The large-component contribution with electrons in the region V_A is evaluated with

$$\begin{aligned} h_{ac,bd}^{P,(AA)} = \sum_{\kappa,\kappa'}\sum_{\ell} & g^{\ell}(j_a\mu_a, j\mu_c)g^{\ell}(j_d\mu_d, j'\mu_b) \\ & \times \int_0^{\infty} dr_2 P_d(r_2)\zeta_b(A,\kappa',\mu_b|r_2) \\ & \times \int_0^{\infty} dr_1 P_a(r_1)\zeta_c(A,\kappa,\mu_c|r_1) r_<^{\ell}/r_>^{\ell+1}, \end{aligned} \tag{27}$$

where $\kappa \leftrightarrow \ell j$, $\kappa' \leftrightarrow \ell' j'$, $r_>(r_<)$ is the larger (smaller) of r_1 and r_2, ζ_b is evaluated for $P_{n_b\kappa_b}$, and ζ_c is evaluated for $P_{n_c\kappa_c}$. The expressions for the small-component integral $h_{ac,bd}^{Q,(AA)}$ as well as $h_{ac,bd}^{(BB)}$ are similar. The integrals $h_{ac,bd}^{(AB)}$ and $h_{ac,bd}^{(BA)}$ are evaluated using the techniques discussed in Sec. III A.

The complexity in evaluating exchange-type integrals is that it includes infinite sums. These sums, however, converge very fast due to the symmetrical reexpansion procedure. It is sufficient to use 15 terms in the expansion of Eq. (27) to obtain exchange-type integrals with an accuracy of 10^{-8} hartree.

IV. RESULTS AND DISCUSSION

A. Ground-state potentials

The ground configuration of the RbCs molecule, formed by one Rb($4p^6 5s$) and one Cs($5p^6 6s$) atom, has three adiabatic relativistic molecular states, the $X\,^1\Sigma^+_{\Omega=0}$ and $a\,^3\Sigma^+_{\Omega=0,1}$ states. A significant part of the binding energy of these states is due to correlation effects. These correlations have a strong dependence on internuclear separation. The basis set of our VB method must accommodate and balance these changing correlations with R.

Experimental studies of the ground $X\,^1\Sigma^+_0$ state of RbCs have been performed by several groups.[32–34] The most recent and precise results, using laser-induced fluorescence combined with Fourier-transform spectroscopy, were obtained in Ref. 34. In addition, authors of Ref. 34 applied the inverted perturbation approach (IPA) to obtain a potential curve for R between $6a_0$ and $25a_0$ and an accurate dissociation energy. Theoretical potentials for the $X\,^1\Sigma^+_0$ and $a\,^3\Sigma^+_{0,1}$ states are given in Ref. 13 over a much wider range of R. Their *ab initio* calculation is based on a nonempirical pseudopotential approach and for the X state is in good agreement with the experimental IPA potential. Our motivation to calculate the ground-state potentials is based on the notion that a pseudopotential approach may lose accuracy for small and large internuclear separations, where no experimental information is available.

In this work we perform a relativistic *all-electron* calculation so that our results do not depend on a pseudopotential. However, we divided the electrons of each atom into two groups: core and valance electrons. Core electrons include electrons from the closed shells $1s^2_{1/2}$, $2s^2_{1/2}$, $2p^2_{1/2}$, $2p^4_{3/2}$,…, up to $4s^2_{1/2}$ for the Rb atom and similarly $1s^2_{1/2}$,…, up to $5s^2_{1/2}$ for the Cs atom. The superscripts denote the number of electrons in the orbital nl_j. Core orbitals do not contribute significantly to the formation of the molecule and excitations out of these shells are, therefore, not included. Nevertheless, these orbitals do define a fully relativistic all-electron core potential for the remaining valence electrons.

Occupied valence electrons are electrons in the $4p^2_{1/2}$, $4p^4_{3/2}$, and $5s_{1/2}$ shells for the Rb atom and $5p^2_{1/2}$, $5p^4_{3/2}$, and $6s_{1/2}$ shells for the Cs atom. Excitations to and from these shells will be allowed. Unlike the core electrons these electrons will play an important role in the formation of the ground electronic state of the RbCs dimer. Despite the fact that the $4p^6$ shell in Rb and $5p^6$ shell in Cs are completely filled, electrons in these shells are called valence electrons as excitations will ensure a proper treatment of "core polarization."

In addition to the two kinds of orbitals, discussed above, unoccupied virtual valence orbitals are used to increase the flexibility of the molecular wave function. Compact Sturm virtual orbitals are used to construct such a basis set. For Rb all unoccupied orbitals are constructed using the energy of the $5s$ valence orbital, while for Cs unoccupied orbitals are based on the $6s$ orbital. Atomic configurations are formed from core and valence orbitals and uniquely labeled by the occupied and unoccupied valence orbitals. For example, the main configuration of the ground state of the Rb atom is $4p^2_{1/2}4p^4_{3/2}5s_{1/2}$ ($=4p^6 5s$), while for the Cs atom it is $5p^6 6s$. The inner-core shells are the same for all configurations and are omitted in this notation.

In addition to the main configuration the calculation of the CI ground-state wave function includes covalent and

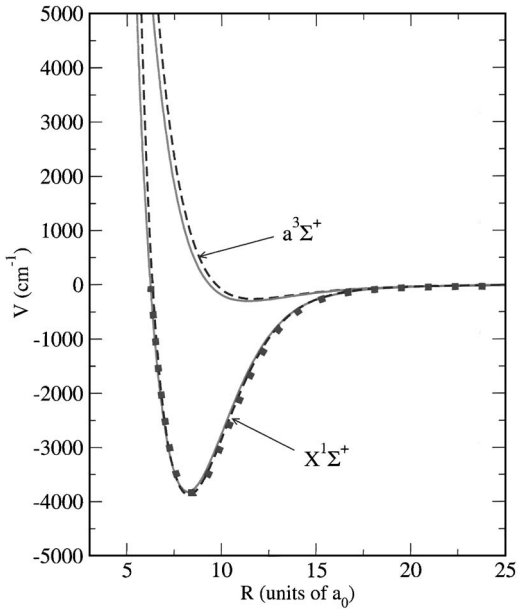

FIG. 2. The ground-state $X\,^1\Sigma_0^+$ and $a\,^3\Sigma_{0,1}^+$ potential-energy curves of RbCs obtained by different methods as function of internuclear separation R. The dotted line corresponds to the IPA potential by Ref. 34, the solid lines are the potentials of the current work, and the dashed lines are potentials by Ref. 13. Table of potential-energy values obtained in this study can be found through EPAPS (Ref. 23).

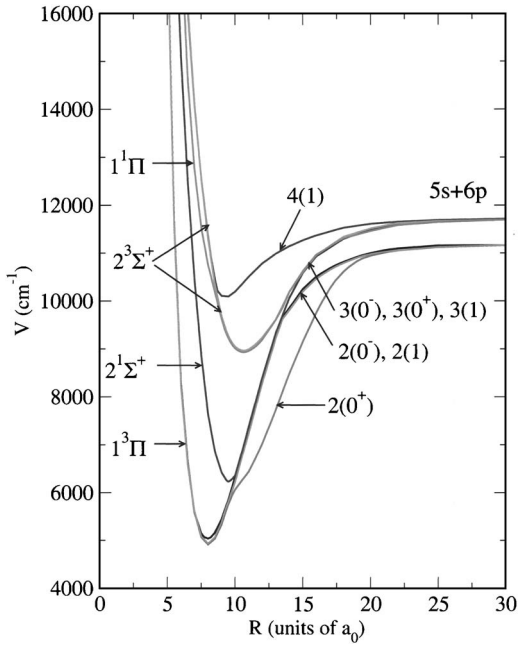

FIG. 3. Electronic potentials of excited states of the RbCs $\Omega=0^{\pm}$ and $\Omega=1$ as function of internuclear separation. Tables of potential-energy values obtained in this study can be found through EPAPS (Ref. 23).

ionic molecular configurations created by the excitation of one or two electrons from $4p^6$ and $5s$ valence shells for Rb and $5p^6$ and $6s$ shells for Cs into higher excited orbitals. We allow excitations up to $n=7$ for Rb and $n=8$ for Cs for $l=0$, 1, and 2. The convergence of the CI expansion can only be determined by increasing the number of configurations in a systematic way. This is achieved by adding atomic orbitals out of which the atomic and thus molecular determinants are constructed. Our best basis set has about 3×10^5 determinants.

Results of our calculation together with data from Refs. 34 and 13 are presented in Fig. 2. The potential energies in this and all other graphs and the table are expressed in units of cm^{-1}, defined through $1\ E_h/hc=219\,475\ \text{cm}^{-1}$, where h is the Planck constant. The comparison of potentials from the three different sources shows that our theoretical potential energies and those of Ref. 13 agree well with the IPA potential for $X\,^1\Sigma_0^+$ for $R\geqslant5a_0$. At shorter R the pseudopotential approach of Ref. 13 gives steeper repulsive walls.

B. Excited-state potentials

We calculated excited potentials with $\Omega=0^{\pm}$ and 1 dissociating to the Rb$(5s)$+Cs$(6p^2P_{1/2,3/2})$ atomic limits, where Ω is the projection of the total electronic angular momentum of the two atoms on the internuclear axis. These attractive potentials are the most likely candidates for use in two-color Raman photoassociation experiments.

The basis set is larger than that used to calculate the ground-state potentials. We added $n=8$, $l=0,1$, orbitals for Rb and $n=9$, $l=0,1$ orbitals for Cs. Moreover, we allow three-electron excitations and occupancy of valence orbitals and two-electron excitations out of the $4p^6$ shell of Rb and $5p^6$ shell of Cs. The main difference with the calculation of the ground-state potentials is the description of the $5p$ orbital of Rb and $6p$ orbital of Cs as a valence orbital. Sturm orbitals are now chosen to mimic either the $5s$ or $5p$ valence orbital for Rb and $6s$ or $6p$ for Cs. That is, for Rb the unoccupied s and d orbitals are constructed using the energy of the $5s$ valence orbital, whereas p orbitals are based on the $5p$ valence orbital. For Cs unoccupied s and d orbitals are based on the $6s$ orbital and p orbitals on the $6p$ orbital. Again covalent and ionic configurations are incorporated in the CI calculation. Unlike the ground-state calculation described in the previous section, the size of the CI matrices is now too large to handle computationally and we are forced to limit the number of determinants. We select determinants based on a perturbative estimate of the correlation coefficient of the excited determinants on the main Rb $4p^65s$+Cs $4p^66p$ configuration. If this coefficient is below a threshold value (10^{-9}) the corresponding excited configuration is omitted from the CI calculation.

Figure 3 shows the relativistic excited-state potentials for RbCs $\Omega=0^{\pm}$ and 1 as a function of internuclear separation. The two dissociation limits in the figure correspond to the fine-structure states of the excited Cs atom plus a ground-state Rb atom. The long-range behavior of the relativistic potentials dissociating to these two limits is attractive and proportional to $1/R^6$. At short internuclear separations $R<7a_0$ the potentials are described by the nonrelativistic Hund's case (a) $n^{2S+1}\Lambda^{\pm}$ labeling. Three avoided crossings are apparent for intermediate internuclear separations. That is, at approximately $8.2a_0$, $10a_0$, and $13.5a_0$. The Hund's case (a) character of the molecular wave function changes rapidly at those R. For example, for the avoided crossing at $8.2a_0$ in Fig. 3 the lower of the two potential curves is to good approximation $a\ 1\ ^1\Pi$ state for $R<8.2a_0$ and $a\ 2\ ^3\Sigma^+$ state for $R>8.2a_0$. For the higher of the two potentials the

TABLE I. Comparison of widths δ_c in cm^{-1} and locations R_c in units of a_0 of avoiding crossings of the excited RbCs potentials calculated here, shown in Fig. 3, and by Fahs *et al.* (Ref. 14). The width of an avoided crossing is defined as the smallest energy separation between the two avoiding potentials.

States	RCI-VB		Fahs *et al.*	
$n(\Omega^{\pm})-m(\Omega^{\pm})$	R_c	δ_c	R_c	δ_c
$2(0^+)-3(0^+)$	10	297	10.1	534
$2(0^-)-3(0^-)$	13.5	273	13.7	208
$2(1)-3(1)$	13.5	205	13.1	148
$3(1)-4(1)$	8.2	240	8.2	43

role of the $2\,^3\Sigma^+$ and $1\,^1\Pi$ states for a fixed R is interchanged. Only states with the same $\Omega^{\pm}$ label avoid each other. At longer R the potentials cannot be labeled by $n^{2S+1}\Lambda^{\pm}$ and only the Hund's case (c) $m(\Omega^{\pm})$ labeling is valid. The numbers n and m indicate the energy-ordered appearance of the states.

The excited potentials of RbCs were previously reported in three other papers.[12–14] The calculations of Refs. 12 and 13 do not include the relativistic effects of the excited states. Calculations performed by Ref. 14 include the spin-orbit interaction by adding a semiempirical spin-orbit pseudopotential to the electrostatic Hamiltonian. Our calculations and those of Ref. 14 are in general agreement. Our $2(0^+)$ potential is on the scale of Fig. 3 wider in the radial direction. This is true for both short and large internuclear separations. Moreover, the bottom of the wells of the curves labeled by $1\,^1\Pi$, $2\,^3\Sigma^+$, and $2\,^1\Sigma^+$ in Fig. 3 is slightly shifted to larger R and deeper in our calculation. The width and location of several of the avoided crossings in Fig. 3 and the corresponding avoided crossings in Ref. 14 are tabulated in Table I. There is a significant difference in the width of the $2(0^+)-3(0^+)$ and $3(1)-4(1)$ avoiding crossings between the two calculations.

C. Permanent dipole moments of the ground and excited states

We have calculated the permanent dipole moments of the RbCs ground-state potentials. The dipole moments are matrix elements of the operator $\mathbf{d}=\Sigma_i Z_i \mathbf{r}_i$, where the sum is over all electrons and nuclei; Z_i and $\mathbf{r}_i$ are the charge and location of particle i, respectively. The matrix elements are over the relativistic multiconfiguration wave functions that result from the CI calculation.

Figure 4 shows the electric dipole moments of the $X\,^1\Sigma^+$ and $a\,^3\Sigma^+$ potentials of RbCs as a function of internuclear separation. The sign convention is such that a negative dipole moment implies that the center of charge of the electrons relative to the center of charge of the two nuclei is displaced towards the Rb atom. At the equilibrium separation of the singlet state the electronic dipole moment is $-1.25(1)$D ($1\ \mathrm{D}=3.336\times10^{-30}$ cm) and at the equilibrium separation of the triplet state 0.06(2)D. The numbers in parentheses are one-standard-deviation uncertainties. The strength of the permanent dipole moments of RbCs is about two times larger than the corresponding dipole moments of KRb.[19] This increase might have been expected given the larger differential

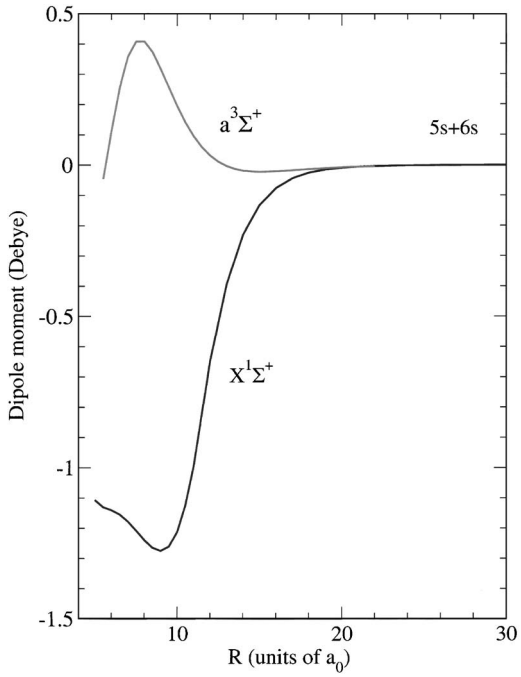

FIG. 4. The electric dipole moments of the $X\,^1\Sigma^+$ and $a\,^3\Sigma^+$ states of RbCs as a function of internuclear separation. Table of electric dipole moments obtained in this study can be found through EPAPS (Ref. 23).

between the ionization energies of Rb and Cs. Nevertheless, the dipole moments are only a fraction of the values for truly polar molecules such as NaCl. The good agreement for the X state between our and two other theoretical determinations[16,15] (within 4% at R_e, the internuclear separation at which the X state has a minimum), obtained by completely different methods, illustrates the reliability of the data.

We find that the distribution of the charge density between Rb and Cs has two contributions. The permanent dipole moments depend not only on the electron charge transfer from Cs to Rb atoms but also on the induced polarization from the charge transfer. Polarization is induced from contributions of the excited unoccupied p and d orbitals. It turns out that the contributions of charge transfer and induced polarization to the dipole moments have opposite sign. We find that the charge transfer is almost equal for the $X\,^1\Sigma^+$ and $a\,^3\Sigma^+$ states, but that the $a\,^3\Sigma^+$ state has a smaller dipole moment.

D. Effect of blackbody radiation on the $X\,^1\Sigma^+$ state

We use the permanent dipole moment of the ground $X\,^1\Sigma^+$ state of RbCs to estimate the lifetime of rovibrational levels in the presence of blackbody radiation. Thermal blackbody radiation due to the surrounding environment has a temperature of about 300 K. The result of the coupling between the molecule and the thermal radiation is that if all population is initially put into one rovibrational state, it, in principle, can rapidly diffuse to other nearby states.

The total radiative transition rate from a rovibrational state can be written as

$$\Gamma^{\mathrm{tot}}_{vlm} = \Gamma^{\mathrm{BB}}_{vlm} + \Gamma^{\mathrm{spont}}_{vlm}, \tag{28}$$

the sum of a blackbody (BB) and a spontaneous-emission (spont) contribution. Photons of the blackbody radiation can be absorbed or emitted by a molecular level. In fact,

$$\Gamma^{\mathrm{BB}}_{vlm} = \sum_{v'l'm'} \bar{n}(\omega_{v'l'})\Gamma^{\mathrm{emis}}(vlm \rightarrow v'l'm') + \sum_{v''l''m''} \bar{n}(\omega_{v''l''})\Gamma^{\mathrm{abs}}(vlm \rightarrow v''l''m'') \tag{29}$$

and

$$\Gamma^{\mathrm{spont}}_{vlm} = \sum_{v',l',m'} \Gamma^{\mathrm{emis}}(vlm \rightarrow v'l'm'), \tag{30}$$

where the indices $v'l'm'$ and $v''l''m''$ denote rovibrational levels with an energy that is smaller and larger than that of vlm, respectively. Equation (30) and the first term of Eq. (29) describe the emission of a photon; the second term of Eq. (29) describes the absorption. The sum over $v''l''m''$ includes the contribution of the continuum of two free atoms as a photon can break the bond of a dimer. The factor $\bar{n}$ corresponds to the average number of photons in an electromagnetic mode at frequency ω and is given by

$$\bar{n}(\omega) = \frac{1}{e^{-\hbar\omega/k_B T} - 1},$$

where $\hbar$ is Planck's constant. Finally, $\hbar\omega_{v'l'}$ denotes the energy difference between $E_{v'l'}$ and E_{vl} and $\hbar\omega_{v''l''}$ denotes the energy difference between $E_{v''l''}$ and E_{vl}.

The emission Γ^{emis} and absorption Γ^{abs} rates that describe the individual contributions are proportional to the square of the vibrationally averaged dipole moment and are given by

$$\Gamma^{\alpha}(vlm \rightarrow v'l'm') = \frac{8\pi}{3}\frac{1}{hc^3}\omega^3 |\langle |d| \rangle|^2, \tag{31}$$

where α is either emis or abs, $\hbar\omega$ is the energy difference of the two rovibrational states vlm and $v'l'm'$, and the rotationally and vibrationally averaged dipole moment $\langle |d| \rangle = \langle v'l'm'|\mathbf{d}(R)\cdot\epsilon|vlm\rangle = \langle v'l'|d(R)|vl\rangle\langle l'm'|C_{1q}(\hat{R})|lm\rangle$, where to good approximation the rovibrational wave function $\langle \mathbf{R}|vlm\rangle = \langle R|vl\rangle Y_{lm}(\hat{R})$, $d(R)$ is the R-dependent dipole moment of either the singlet or triplet potential, ϵ is the photon polarization, $Y_{lm}(\hat{R}) = \sqrt{(2l+1)/(4\pi)}C_{lm}(\hat{R})$ is a spherical harmonic, $\hat{R}$ is the orientation of the intermolecular axis in the space-fixed coordinate system, and $q = m - m'$. The selection rules of the vibrationally averaged dipole moment ensure $|l-l'| \leq 1$ and $|m-m'| \leq 1$.

The wave functions $\langle R|vl\rangle$ and energies are obtained for the potential $V_X(R) + \hbar^2 l^2/(2\mu R^2)$, where $V_X(R)$ is the $X\,^1\Sigma^+$ potential and μ is the reduced molecular mass. We evaluate the rovibrational wave functions using a discrete variable representation (DVR) for the Schrödinger equation.[35] The vibrationally averaged dipole moment is the overlap between the wave functions and the R-dependent permanent dipole moment. For the discretization a hard wall is placed at large internuclear separation. We have checked that moving the hard wall to larger R and increasing the number of discretization points do not change our results.

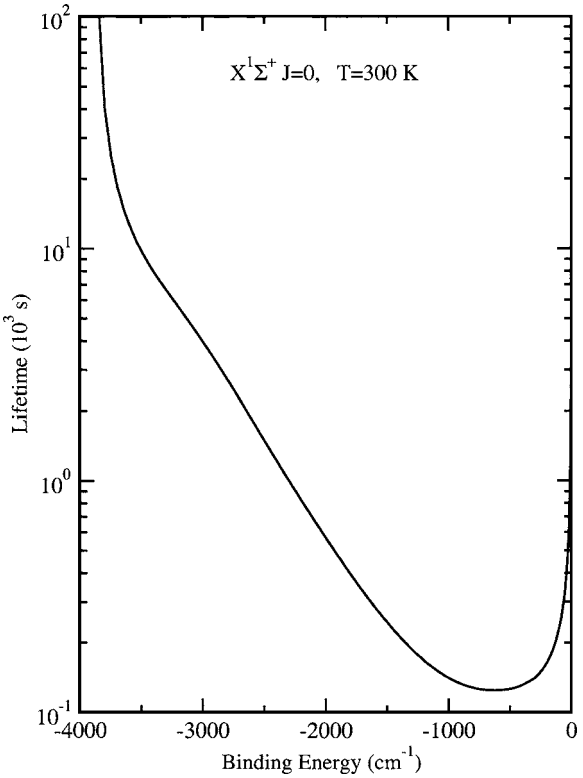

FIG. 5. The $T=300$ K blackbody lifetime of $J=0$ vibrational levels of the $X\,^1\Sigma^+$ state of RbCs as a function of their binding energy.

Figure 5 shows the partial lifetimes $1/\Gamma^{\mathrm{BB}}_{vlm}$ of the $X\,^1\Sigma^+ \cdot l=0$ vibrational states as a function of their binding energy for $T=300$ K. For this temperature spontaneous lifetimes are much larger than the blackbody lifetimes and are not shown in the figure. The graph also shows that the lowest and highest vibrational levels live longer in the presence of blackbody radiation. At room temperature the shortest lifetimes (130 s) occur for vibrational levels between $v=80$ and 85 and binding energies between $E/(hc) = -550$ and -650 cm^{-1}. This lifetime is much longer than the typical duration of ultracold experiments.

E. Transition dipole moments

The relativistic multiconfiguration molecular wave functions have also been used to calculate the transition electric dipole moments between the $^{1,3}\Sigma^+$ states of the ground configuration and $\Omega = 0^{\pm}, 1$ components of excited $^{1,3}\Sigma^+$ and $^{1,3}\Pi$ states dissociating to the $5s+6p$ limits. In the future these data will help provide information about the most efficient scheme for forming a RbCs molecule in the singlet $X\,^1\Sigma^+$ ground state from a collision of ultracold Rb and Cs. Figures 6 and 7 show some of the nonzero transition dipole moments from the $X\,^1\Sigma^+$ and $a\,^3\Sigma^+$ states to excited states. At long range the transition dipole moments are independent of R and their absolute values approach the Cs $6s \rightarrow 6p$ (^2P_j) transition dipole moments.

At short-range internuclear separation the dipole moments strongly depend on R. This behavior reflects the

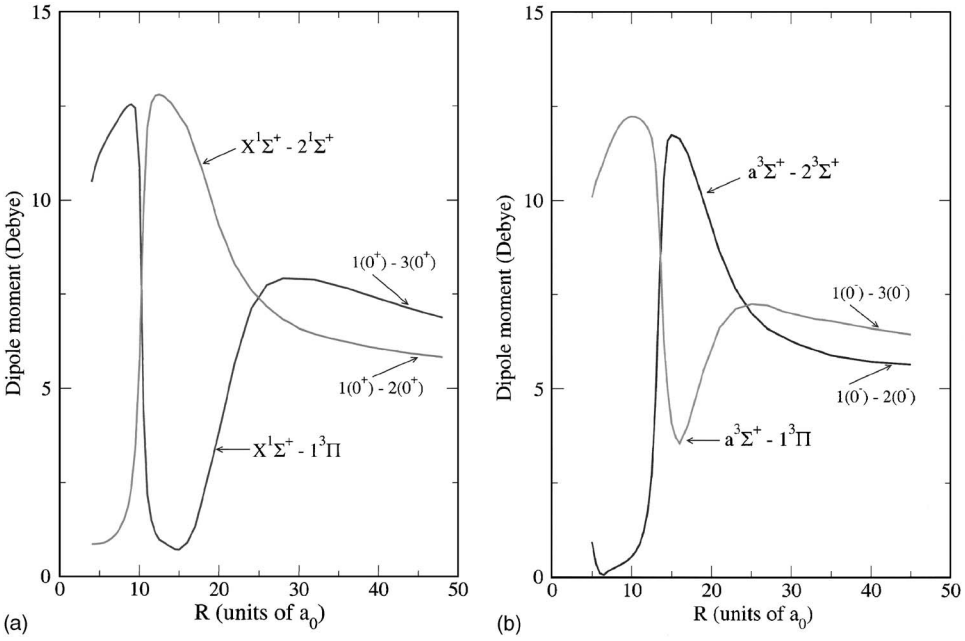

FIG. 6. Absolute values of transition dipole moments from the $X\ ^1\Sigma^+$ (left panel) and from the $a\ ^3\Sigma^+$ (right panel) ground states to excited states of RbCs as a function of internuclear separation. The curves are labeled by short-range and long-range symmetries. The short-range labeling is only valid where the arrows touch the curve. Indeed, for example, for the right panel the curve labeled $a\ ^3\Sigma^+ - 2\ ^3\Sigma^+$ around $17a_0$ is better labeled by $a\ ^3\Sigma^+ - 1\ ^3\Pi$ for $R < 10a_0$. For the other curve in this panel the correlation is inverted. Tables of transition dipole moments obtained in this study can be found through EPAPS (Ref. 23).

change from a Hund's case (a) to a relativistic coupling scheme between $20a_0$ and $30a_0$. The sudden change in dipole moments in Figs. 6 and 7 near $10a_0$, $13.5a_0$, and $8.2a_0$ correlates with avoided crossings between the $\Omega = 0^+$, 0^-, and 1 components of the $1\ ^3\Pi$, $2\ ^1\Sigma^+$, $2\ ^3\Sigma^+$, and $1\ ^1\Pi$ potentials, shown in Fig. 3. The triplet $a\ ^3\Sigma^+$ to triplet $1\ ^3\Pi$ transition dipole moment at short internuclear separations is small as can be understood by noting that the potentials at these separations are similar in nature to that of a homonuclear alkali-metal dimer, where *gerade/ungerade* symmetry is valid and transitions between $a\ ^3\Sigma_u^+$ and $1\ ^3\Pi_u$ states are forbidden. We estimate that the uncertainty of the transition dipole moments is 0.3 D based on a comparison of the dipole moments at $R = 100a_0$ with the experimental dipole moments of the Cs atom.[36]

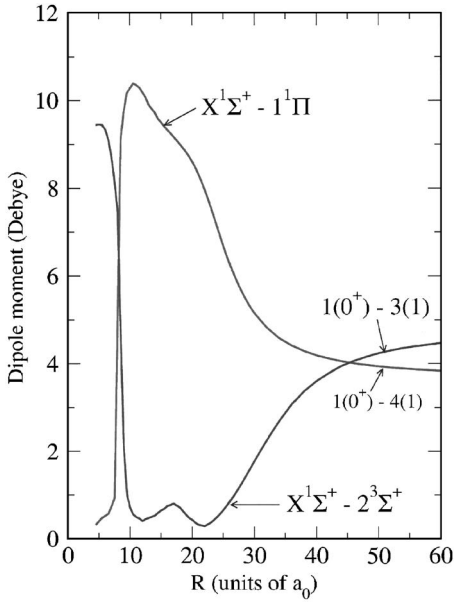

FIG. 7. Absolute values of transition dipole moments from the $X\ ^1\Sigma^+$ ground to $\Omega = 1$ excited states of RbCs as a function of internuclear separation. The curves are labeled by approximate short-range ($^{2S+1}\Lambda$) symmetries and exact relativistic ($\Omega^\pm$) symmetries. Tables of transition dipole moments obtained in this study can be found through EPAPS (Ref. 23).

V. CONCLUSION

We have reported on an *ab initio* relativistic study of alkali-metal RbCs molecule, relevant for photoassociation experiments and for the precise control of ultracold-atomic systems placed in a trap or an optical lattice.

We have calculated potential-energy curves and transition dipole moments to excited states dissociating to $Rb(5s)+Cs(6s)$ and $Rb(5s)+Cs(6p)$ atomic limits. It was shown that the sudden changes in dipole moments as functions of R are related to avoided crossings between appropriate electronic potentials. Our quantitative determination of the RbCs transition electric dipole moments is the first step towards obtaining photoabsorption and molecular production rates in an ultracold gas of Rb and Cs atoms.

In addition, we determined the permanent dipole moments of the $^{1,3}\Sigma^+$ states of the ground configuration of the RbCs heteronuclear molecule, which show impressive agreement with other calculations[16,15] obtained by alternative computational methods.

We have investigated the effect of blackbody radiation on the dipolar RbCs molecule by evaluating Franck-Condon factors between vibrational levels of the ground state. It is shown that the shortest lifetime is around 130 s which is much longer than the duration of typical ultracold-atom experiments, so that this effect can be ignored.

There remain open questions about the spin-orbit effects in the molecular structure of RbCs. The spin-orbit coupling between the $A\ ^1\Sigma^+$ and $b\ ^3\Pi$ as well as the $^3\Sigma^+$ and $^1\Pi$ excited states plays a crucial role in the spectroscopy of any alkali-metal dimers. Until now this coupling was modeled by *ad hoc* R-dependent functions adjusted to fit experimental data on vibrational energies of the potentials. In the heavy RbCs molecule the effect of the spin-orbit coupling is expected to be large. We have started to calculate spin-orbit

functions for several excited potentials in order to provide an explanation for its functional behavior.

ACKNOWLEDGMENTS

This work was supported by the Army Research Office. We acknowledge useful discussions with Professor T. Bergeman and Professor M. Lyyra.

[1] D. DeMille, Phys. Rev. Lett. **88**, 067901 (2002).
[2] M. Olshanii, Phys. Rev. Lett. **81**, 938 (1998); D. S. Petrov and G. V. Shlyapnikov, Phys. Rev. A **64**, 012706 (2001); U. Al Khawaja, J. O. Andersen, N. P. Proukakis, and H. T. C. Stoof, *ibid.* **66**, 013615 (2002); E. Bodo, F. Gianturco, and A. Dalgarno, J. Chem. Phys. **116**, 9222 (2002); D. S. Petrov, M. A. Baranov, and G. V. Shlyapnikov, Phys. Rev. A **67**, 031601 (2003); B. Damski, L. Santos, E. Tiemann, M. Lewenstein, S. Kotochigova, P. Julienne, and P. Zoller, Phys. Rev. Lett. **90**, 110401 (2003).
[3] A. J. Kerman, J. M. Sage, S. Sainis, T. Bergeman, and D. DeMille, Phys. Rev. Lett. **92**, 033004 (2004).
[4] D. Wang, J. Qi, M. F. Stone, O. Nikolayeva, H. Wang, B. Hattaway, S. D. Gensemer, P. L. Gould, E. E. Eyler, and W. C. Stwalley, Phys. Rev. Lett. **93**, 243005 (2005).
[5] A. N. Nikolov, J. R. Ensher, E. E. Eyler, H. Wang, W. C. Stwalley, and P. L. Gould, Phys. Rev. Lett. **84**, 246 (2000).
[6] M. W. Mancini, G. D. Telles, A. R. L. Caires, V. S. Bagnato, and L. G. Marcassa, Phys. Rev. Lett. **92**, 133203 (2004).
[7] S. Kotochigova, E. Tiesinga, and P. S. Julienne, Eur. Phys. J. D **31**, 189 (2004).
[8] D. Wang, J. Qi, M. F. Stone *et al.*, Eur. Phys. J. D **31**, 165 (2004).
[9] W. C. Stwalley, Eur. Phys. J. D **31**, 221 (2004).
[10] T. Bergeman, A. J. Kerman, J. Sage, S. Sainis, and D. DeMille, Eur. Phys. J. D **31**, 179 (2004).
[11] S. Azizi, M. Aymar, and O. Dulieu, Eur. Phys. J. D **31**, 195 (2004).
[12] D. Pavolini, T. Gustavsson, F. Spiegelmann, and J.-P. Daudey, J. Phys. B **22**, 1721 (1989).
[13] A. R. Allouche, M. Korek, K. Fakherddin, A. Chaalan, M. Dagher, F. Taher, and M. Aubert-Frecon, J. Phys. B **33**, 2307 (2000).
[14] H. Fahs, A. R. Allouche, M. Korec, and M. Aubert-Frecon, J. Phys. B **35**, 1501 (2002).
[15] G. Igel-Mann, U. Wedig, P. Fuentealba, and H. Stoll, J. Chem. Phys. **84**, 5007 (1986).
[16] M. Aymar and O. Dulieu, J. Chem. Phys. **122**, 204302 (2005).
[17] S. Kotochigova, E. Tiesinga, and I. Tupitsyn, *New Trends in Quantum Systems in Chemistry and Physics* (Kluwer Academic, The Netherlands, 2001), Vol. 1, pp. 219–242.
[18] S. Kotochigova, E. Tiesinga, and P. S. Julienne, Phys. Rev. A **63**, 012517 (2000).
[19] S. Kotochigova, P. S. Julienne, and E. Tiesïnga, Phys. Rev. A **68**, 022501 (2003).
[20] E. Tiesinga, S. Kotochigova, and P. S. Julienne, Phys. Rev. A **65**, 042722 (2002).
[21] S. Kotochigova and P. S. Julienne, *Potential Energy Surface Database of Group II Dimer Molecules* (National Institute of Standards and Technology, Gaithersburg, MD, 2003); in http://physics.nist.gov/PhysRefData/PES
[22] T. Bergeman, C. Fellows, R. Gutters, and C. Amiot, Phys. Rev. A **67**, 050501 (2003).
[23] See EPAPS Document No. E-JCPSA6-123-305539 for html files containing numerical data of results obtained in our calculations. This document can be reached via a direct link in the online article's HTML reference section or via the EPAPS homepage (http://www.aip.org/pubservs/epaps.html).
[24] I. I. Tupitsyn, Russ. J. Phys. Chem. **74**, 304 (2000).
[25] I. P. Grant, Adv. Phys. **19**, 747 (1970).
[26] V. A. Fock, *The Principles of Quantum Mechanics*, 2nd ed. (Nauka, Moskow, 1976).
[27] P. P. Pavinsky and A. I. Shestyuk, *Problems of Theoretical Physics* (Leningrad University Press, 1974), Pt. 1, pp. 66–107.
[28] R. Szmykowski, J. Phys. B **30**, 825 (1997).
[29] I. P. Grant and H. M. Quiney, Phys. Rev. A **62**, 022508 (2000).
[30] I. I. Tupitsyn and A. V. Loginov, Opt. Spectrosc. **94**, 319 (2003).
[31] P. O. Löwdin, Adv. Phys. **5**, 1 (1956).
[32] H. Kato and H. Kobayashi, J. Chem. Phys. **79**, 123 (1983).
[33] T. Gustavsson, C. Amiot, and J. Verges, Mol. Phys. **64**, 279 (1988).
[34] C. Fellows, R. Gutters, A. Campos, J. Verg'es, and C. Amiot, J. Mol. Spectrosc. **197**, 19 (1999).
[35] R. Meyer, J. Chem. Phys. **52**, 2053 (1970); D. T. Colbert and W. H. Miller, *ibid.* **96**, 1982 (1992); O. Dulieu and P. S. Julienne, *ibid.* **103**, 60 (1995).
[36] http://physics.nist.gov/PhysRefData/contents-atomic.html